Available online at www.sciencedirect.com
SCIENCE DIRECT®
Comput. Methods Appl. Mech. Engrg. 192 (2003) 2223–2248
Computer methods in applied mechanics and engineering
www.elsevier.com/locate/cma

Improved implicit integrators for transient impact problems—dynamic frictional dissipation within an admissible conserving framework

G.R. Love, T.A. Laursen *

Department of Civil and Environmental Engineering, 127 Hudson Hall, P.O. Box 90287, Duke University, Durham, NC 27708-0287, USA

Received 14 May 2002; received in revised form 26 November 2002

Abstract

This work presents a frictional extension of an improved conservative integration framework for dynamic contact, extending the details of the frictionless scheme to encompass Coulomb stick/slip friction and the associated conservation/dissipation. It addresses algorithmic details that do not appear in the frictionless context, establishing an appropriate and objective treatment of relative tangential motion that is necessary to rigorously ensure conservation of angular momentum in the fully discrete setting. It also further extends the functionality of a *discrete contact velocity* term proposed in the frictionless implementation, using it to preserve conservation or dissipation locally as warranted by the frictional model and effectively enabling an enforcement of the contact constraints independent of energy considerations. The result is a robust implicit algorithmic framework for dynamic frictional impact, viable for large deformation analysis, appropriately conservative or dissipative for both stick and slip phenomena on a local scale, and readily extensible to more complex frictional models.

1. Introduction

There exists currently a growing body of computational work in non-linear dynamics that utilizes a class of *conservative* integration methods, i.e. methods that are designed to better emulate a given physical system by algorithmically preserving a particular set of physically motivated quantities *by construction*. One such method, introduced for elastodynamics by Simo and Tarnow [16] and generalized by Gonzalez [8], establishes a means of preserving algorithmic versions of the system energy as well as the linear and angular momenta over a discretized bulk continuum. The method is well conceived, as energy is often the defining metric for determining numerical stability in a system, and a number of sources [6,8] have demonstrated the possibility of 'instability', in the form of boundless energy growth, that can result from an ad hoc

* Corresponding author. Tel.: +1-919-660-5430; fax: +1-919-660-5219.
E-mail address: laursen@duke.edu (T.A. Laursen).

0045-7825/03/$ - see front matter
doi:10.1016/S0045-7825(03)00257-3

application or extension of a traditional linear integration method to a system with even relatively simple non-linearities.

The non-linearities associated with dynamic impact are relatively complex, even given the simplest mathematical description. In the most basic form a contact problem must define or determine the time of initial contact and release for each of a potentially changing but common set of surface points on a pair of colliding bodies, and also consider the magnitudes and directions of any associated contact effects, all of which are generally unknown and characterized by both spatial and temporal discontinuities. The contact entities themselves are also heavily influenced by the associated bulk media, and successful description of the former necessitates a careful consideration of the latter. A few contact descriptions, notably Armero and Petocz [1], Laursen and Chawla [10], Demkowicz and Bajer [7], and Laursen and Love [11], have chosen to consider frictionless dynamic impact under the auspices of a conservative system, extending the framework to incorporate the conserving mathematical idealization of a frictionless surface interaction.

It might seem a contradiction of sorts to extend such algorithms to the realm of physically *dissipative* phenomena, whose presence tends to 'naturally' stabilize their respective systems and appears to obviate the need for a conserving application. Developments in the interest of controlling numerical dissipation (e.g. [3,4]) lead to the conclusion that, given suitable a priori energy estimates for the effects of a given dissipative phenomena, it is possible to accurately render these effects by capturing the dissipative values within a conservative context, free from the parameter-dependent numerical dissipation inherited from traditional temporal integration schemes. This approach has been recently applied to bulk elastoplasticity in such works as Meng and Laursen [14] and has been advocated for friction by both Armero and Petocz [2], and Chawla and Laursen [5] as extensions of their respective frictionless works.

These frictional extensions, however, make the same concessions as their respective frictionless foundations in the treatment of the contact interface. As discussed in Laursen and Love [11], the method of Laursen and Chawla [10] partially compromises the normal contact constraints in the interest of making a consistent accounting of system energy. In retaining this discrete overlap through the frictional extension, Chawla and Laursen [5] are forced to concede algorithmic conservation of angular momentum for frictional traction, in large part due to the unfortunate selection of non-invariant algorithmic description for the relative tangential motion. Armero and Petocz [2] do maintain conservation of momenta through a more judicious frame-indifferent discretization of the tangential rate terms, but retain the algorithmic artifacts of their frictionless case, namely a localized storage of non-physical surface energy in the regularization potential and the associated caveat that complete energy balance is only achieved upon full release of the contact constraints. In addition, their treatment of frictional energy change only adheres to the continuum estimate of energy dissipation in a qualitative sense, ensuring a consistently dissipative treatment over the course of a contact event, but not quantifying the dissipation in relation to the established a priori estimates.

In Laursen and Love [11], we treated the frictionless impact problem by using a *discrete contact velocity* term as a means of resolving conservation of energy without placing undue constraint on the normal contact forces. In this extension to frictional problems, we will show that with careful discretization of a frictional system, it is possible to apply the discrete contact velocity framework so that the discrete system not only conserves both linear and angular momentum, but respectively conserves or dissipates energy appropriate to the local frictional phenomenon. The energy dissipation is quantitatively established by a direct discretization of the continuum dissipation estimates, thus correctly capturing physical dissipation in the regularization limit.

Section 2 provides the notational foundation for the subsequent algorithmic development, outlining the virtual work description and contact kinematics for generalized dynamic contact with Coulomb friction. The continuum system is then systematically discretized in Sections 3.1 and 3.2, culminating with the addition of the discrete velocity update in Section 3.3. The remaining portions of Section 3 describe the algorithmic details necessary to ensure momentum conservation and consistent energy dissipation (Sections 3.4 and 3.5

respectively), outline a regularization of the discrete constraints (Section 3.6), and provide a summary of the process. The numerical examples of Section 4 demonstrate the situationally dependent conservative/dissipative behavior captured by the algorithm for a sampling of dynamic frictional impact problems.

2. Consistent impact systems

This section establishes our notation for the equations governing the contact of solids, with extensive consideration of the continuum formulation of large deformation contact as described by Laursen and Simo [12] and extrapolated in frictional investigations by both Chawla and Laursen [5], and Armero and Petocz [2]. Although a Coulomb law is presented here, the subsequent algorithmic development should be sufficiently general as to be extensible to more complex frictional contact models.

2.1. The virtual work description

To begin, we define open sets $\Omega^{(i)} \subset \mathbb{R}^{n_{\mathrm{sd}}}$, $i = \{1,2\}$, $n_{\mathrm{sd}} = \{1,2,3\}$, to denote reference configurations of two bodies with boundaries $\partial\Omega^{(i)}$ individually subdivided into non-intersecting regions $\Gamma_\sigma^{(i)}$ (Neumann boundary), $\Gamma_\varphi^{(i)}$ (Dirichlet boundary), and $\Gamma_{\mathrm{c}}^{(i)}$ (contact boundary), each invariant with time and satisfying

$$\Gamma_\sigma^{(i)} \cup \Gamma_\varphi^{(i)} \cup \Gamma_{\mathrm{c}}^{(i)} = \partial\Omega^{(i)}. \tag{1}$$

Given time interval $\mathbb{I} \equiv [0,T]$, and appropriate spaces for admissible deformations $\boldsymbol{\varphi}_t^{(i)}$ and admissible variational functions $\overset{*}{\boldsymbol{\varphi}}{}^{(i)}$, the weak form of the dynamic contact problem can be thus expressed for each body (i):

Find $\boldsymbol{\varphi}_t^{(i)}$ such that for all $\overset{*}{\boldsymbol{\varphi}}{}^{(i)}$:

$$\langle (\rho_0 \dot{\boldsymbol{V}}_t - \boldsymbol{f}_t), \overset{*}{\boldsymbol{\varphi}} \rangle^{(i)} + \langle D\boldsymbol{\varphi}_t \boldsymbol{S}_t, \mathrm{GRAD}[\overset{*}{\boldsymbol{\varphi}}] \rangle^{(i)} - \langle \bar{\boldsymbol{t}}_t, \overset{*}{\boldsymbol{\varphi}} \rangle_{\Gamma_\sigma}^{(i)} = \langle \boldsymbol{t}_t, \overset{*}{\boldsymbol{\varphi}} \rangle_{\Gamma_{\mathrm{c}}}^{(i)}. \tag{2}$$

In (2) and throughout we make use of a shorthand description of integral products,

$$\int_{\Omega^{(i)}} (\bullet) \cdot (\bullet)\, \mathrm{d}\Omega^{(i)} := \langle \bullet, \bullet \rangle^{(i)} \quad \text{and} \quad \int_{\Gamma^{(i)}} (\bullet) \cdot (\bullet)\, \mathrm{d}\Gamma^{(i)} := \langle \bullet, \bullet \rangle_{\Gamma}^{(i)}. \tag{3}$$

Values in (2) include reference density, ρ_0; local material velocities, $\boldsymbol{V}_t = \dot{\boldsymbol{\varphi}}_t$; and a representation of the second (symmetric) Piola–Kirchhoff stress, denoted $\boldsymbol{S}_t$. Herein we consider an *unforced* system, with constant zero values for prescribed body force $(\boldsymbol{f}_t)$ and boundary traction $(\bar{\boldsymbol{t}}_t)$, and no imposed boundary displacements $(\Gamma_\varphi^{(i)} = \emptyset)$. The unprescribed contact surface tractions $(\boldsymbol{t}_t)$ are typically described through a set of spatial geometric constraints dependent upon the unknown deformation mappings $\boldsymbol{\varphi}_t^{(i)}$.

The variational form in (2) is composed of integral *virtual work* functions with the left hand side, summed over each of the i contacting bodies, representing the total virtual work of the combined non-contact forces on the system,

$$G(\boldsymbol{\varphi}_t, \overset{*}{\boldsymbol{\varphi}}) := \sum_i^2 \left[\langle \rho_0 \dot{\boldsymbol{V}}_t, \overset{*}{\boldsymbol{\varphi}} \rangle^{(i)} + \langle D\boldsymbol{\varphi}_t \boldsymbol{S}_t, \mathrm{GRAD}[\overset{*}{\boldsymbol{\varphi}}] \rangle^{(i)} \right]. \tag{4}$$

We use a standard Lagrangian description for the contact surfaces, designating the material points as $\boldsymbol{X} \in \Gamma_{\mathrm{c}}^{(1)}$ and $\boldsymbol{Y} \in \Gamma_{\mathrm{c}}^{(2)}$, respectively. Quantities on $\Gamma_{\mathrm{c}}^{(2)}$ are mapped from $\Gamma_{\mathrm{c}}^{(1)}$ through a *closest point projection* minimization

$$\overline{\boldsymbol{Y}}(\boldsymbol{X},t) := \arg\min_{\boldsymbol{Y}\in\Gamma_{\mathrm{c}}^{(2)}} \left\|\boldsymbol{\varphi}_t^{(1)}(\boldsymbol{X}) - \boldsymbol{\varphi}_t^{(2)}(\boldsymbol{Y})\right\|. \tag{5}$$

Summing the right hand side of (2) and establishing force balance ($\boldsymbol{t}^{(1)} = -\boldsymbol{t}^{(2)} := \boldsymbol{t}$) along the shared contact surface ($\Gamma_{\mathrm{c}}^{(1)} = \Gamma_{\mathrm{c}}^{(2)} := \Gamma_{\mathrm{c}}$), yields a single integral expression for the *virtual work of contact*:

$$G_{\mathrm{c}}(\boldsymbol{\varphi}_t, \overset{*}{\boldsymbol{\varphi}}) := -\left\langle \boldsymbol{t}, \left[\overset{*}{\boldsymbol{\varphi}}{}^{(1)}(\boldsymbol{X}) - \overset{*}{\boldsymbol{\varphi}}{}^{(2)}(\overline{\boldsymbol{Y}}(\boldsymbol{X},t))\right]\right\rangle_{\Gamma_{\mathrm{c}}}. \tag{6}$$

The contact problem is thus compactly stated in virtual work terms:

Find $\boldsymbol{\varphi}_t^{(i)}$, subject to the contact constraints, such that for all $\overset{*}{\boldsymbol{\varphi}}{}^{(i)}$:

$$G(\boldsymbol{\varphi}_t, \overset{*}{\boldsymbol{\varphi}}) + G_{\mathrm{c}}(\boldsymbol{\varphi}_t, \overset{*}{\boldsymbol{\varphi}}) = 0. \tag{7}$$

2.2. Definitions on the contact surface

We decompose (5) into a unit direction vector $\boldsymbol{v}$ aligned with the contact surface normal on $\Gamma_{\mathrm{c}}^{(2)}$ and with a *gap function* magnitude, g,

$$\boldsymbol{\varphi}_t^{(1)}(\boldsymbol{X}) - \boldsymbol{\varphi}_t^{(2)}(\overline{\boldsymbol{Y}}(\boldsymbol{X},t)) = -g\boldsymbol{v}; \tag{8}$$

and adopt the convention whereby $\boldsymbol{v}$ is directed *outward* of $\Omega^{(2)}$ such that the 'gap' is *negative* ($g < 0$) for admissible (i.e. non-penetrated) deformations. Manipulation of (8) defines a geometric description of the gap magnitude,

$$g = -\boldsymbol{v}\cdot\left(\boldsymbol{\varphi}_t^{(1)}(\boldsymbol{X}) - \boldsymbol{\varphi}_t^{(2)}(\overline{\boldsymbol{Y}}(\boldsymbol{X},t))\right). \tag{9}$$

Following Laursen and Simo [12], we parameterize of the projection contact surface ($\Gamma_{\mathrm{c}}^{(2)}$) in reference variables ξ^{α}, ($\alpha = 1, n_{\mathrm{sd}} - 1$), and derive $n_{\mathrm{sd}} - 1$ spatial vectors $\boldsymbol{\tau}_{\alpha}$ through differentiation of (8) within this parameterization, maintaining the closest-point minimization (indicated with the overbar notation) such that

$$\boldsymbol{\tau}_{\alpha} := \boldsymbol{\varphi}_{t,\alpha}^{(2)}(\bar{\xi}(\boldsymbol{X},t)). \tag{10}$$

Through this derivative definition, the tangential vectors $\boldsymbol{\tau}_{\alpha}$ are orthogonal to the surface normal $\boldsymbol{v}$, however, the resulting convected basis will not in general represent an orthonormal space, and requires consideration of the associated metric and its inverse,

$$m_{\alpha\beta} := \boldsymbol{\tau}_{\alpha}\cdot\boldsymbol{\tau}_{\beta}, \quad [m^{\alpha\beta}] = [m_{\alpha\beta}]^{-1}, \tag{11}$$

in order to define the dual basis,

$$\boldsymbol{\tau}^{\alpha} := m^{\alpha\beta}\boldsymbol{\tau}_{\beta}. \tag{12}$$

(note that here the summation convention is implied on repeated indices). The contact forces, $\boldsymbol{t}$, can now be decomposed in terms of normal and tangential parts, with respective normal (t_{N}) and tangential ($t_{\mathrm{T}_{\alpha}}$) magnitudes, i.e.

$$\boldsymbol{t} = t_{\mathrm{N}}\boldsymbol{v} - t_{\mathrm{T}_{\alpha}}\boldsymbol{\tau}^{\alpha}. \tag{13}$$

Variations of the important surface quantities, namely the gap function g and the projected surface parameterization $\bar{\xi}$, can be generated as directional derivatives aligned with deformation variation $\overset{*}{\boldsymbol{\varphi}}$. Consider

$$\delta g = -\boldsymbol{v}\cdot\left[\overset{*}{\boldsymbol{\varphi}}{}^{(1)}(\boldsymbol{X}) - \overset{*}{\boldsymbol{\varphi}}{}^{(2)}(\overline{\boldsymbol{Y}}(\boldsymbol{X},t))\right] \tag{14}$$

and

$$A_{\alpha\beta}\,\delta\bar{\xi}^{\alpha} = \boldsymbol{\tau}_{\beta}\cdot\left[\overset{*}{\boldsymbol{\varphi}}{}^{(1)}(\boldsymbol{X}) - \overset{*}{\boldsymbol{\varphi}}{}^{(2)}(\overline{\boldsymbol{Y}}(\boldsymbol{X},t))\right] + g\boldsymbol{v}\cdot\left[-\overset{*}{\boldsymbol{\varphi}}{}^{(2)}_{,\beta}(\overline{\boldsymbol{Y}}(\boldsymbol{X},t))\right], \tag{15}$$

where the symmetric matrix $A_{\alpha\beta}$ and its inverse $A^{\alpha\beta}$ are defined as

$$A_{\alpha\beta} := m_{\alpha\beta} + g\boldsymbol{v}\cdot[\boldsymbol{\varphi}^{(2)}_{t,\alpha\beta}(\overline{\boldsymbol{Y}}(\boldsymbol{X},t))] \quad \text{and} \quad [A^{\alpha\beta}] := [A_{\alpha\beta}]^{-1}. \tag{16}$$

Temporal derivatives (denoted with a superimposed dot) are calculated in the same manner, yielding a local description for a *gap rate*, $v_{\mathrm{N}} = \dot{g}$ and local measures of relative tangential motion, or *slip rates*, $v^{\alpha}_{\mathrm{T}} = \dot{\bar{\xi}}^{\alpha}$ in terms of material velocities $\boldsymbol{V}^{(i)} = \dot{\boldsymbol{\varphi}}^{(i)}_{t}$:

$$v_{\mathrm{N}} = \dot{g} = -\boldsymbol{v}\cdot[\boldsymbol{V}^{(1)}(\boldsymbol{X}) - \boldsymbol{V}^{(2)}(\overline{\boldsymbol{Y}}(\boldsymbol{X},t))] \tag{17}$$

and

$$A_{\alpha\beta}v^{\alpha}_{\mathrm{T}} = A_{\alpha\beta}\dot{\bar{\xi}}^{\alpha} = \boldsymbol{\tau}_{\beta}\cdot[\boldsymbol{V}^{(1)}(\boldsymbol{X}) - \boldsymbol{V}^{(2)}(\overline{\boldsymbol{Y}}(\boldsymbol{X},t))] + g\boldsymbol{v}\cdot[-\boldsymbol{V}^{(2)}_{,\beta}(\overline{\boldsymbol{Y}}(\boldsymbol{X},t))]. \tag{18}$$

The slip rates can then be used in the definition of a relative and frame indifferent *slip velocity* as proposed in Laursen and Simo [12]. In this case we facilitate our development with a notably different constitutive decision and opt for a completely spatial definition of the slip velocity through use of the *spatial* metric $m_{\alpha\beta}$. Consider the definition

$$\boldsymbol{v}_{\mathrm{T}} := v^{\beta}_{\mathrm{T}}\boldsymbol{\tau}_{\beta} = m_{\alpha\beta}v^{\beta}_{\mathrm{T}}\boldsymbol{\tau}^{\alpha}. \tag{19}$$

The descriptions in (14) and (15) are now combined with the contact force decomposition (13) and substituted into the variational equation to elicit a new description for the virtual work of contact in terms of the surface variations,

$$G_{\mathrm{c}}(\boldsymbol{\varphi}_{t}, \overset{*}{\boldsymbol{\varphi}}) = \int_{\Gamma_{\mathrm{c}}} [t_{\mathrm{N}}\,\delta g + t_{\mathrm{T}_{\alpha}}\,\delta\bar{\xi}^{\alpha}]\,\mathrm{d}\Gamma_{\mathrm{c}}. \tag{20}$$

The equivalence of (6) and (20) rests upon a pair of *complementarity conditions*,

$$t_{\mathrm{N}}g = 0 \quad \text{and} \quad t_{\mathrm{T}_{\alpha}}g = 0, \tag{21}$$

which establish that the contact force magnitudes (non-zero only during contact) and the gap functions g (negative only when *out* of contact) cannot be mutually non-zero in the continuum description. The dilitational components of the tangential variation (the last term in each of (15) and (16)) can thus be considered as zero over the contact surfaces, validating the virtual work description (20).

2.3. Contact constraints

We apply a standard set of Kuhn–Tucker conditions in terms of the kinematic geometry, first in the normal direction, which remains the same for both frictionless and frictional contact:

$$\begin{aligned} &g \leqslant 0,\\ &t_{\mathrm{N}} \geqslant 0,\\ &t_{\mathrm{N}}g = 0,\\ &t_{\mathrm{N}}v_{\mathrm{N}} = 0. \end{aligned} \tag{22}$$

The tangential constraints are governed by a particular choice of frictional law, chosen here as classical Coulomb friction and governed by defining a relationship between the slip velocity as defined in (19) and the Euclidean normalized ($\|\cdot\|$) tangential portion of the contact force vector, $\boldsymbol{t}_{\mathrm{T}} = t_{\mathrm{T}_{\alpha}}\boldsymbol{\tau}^{\alpha}$, where

$$\boldsymbol{v}_{\mathrm{T}} = \zeta \frac{\boldsymbol{t}_{\mathrm{T}}}{\|\boldsymbol{t}_{\mathrm{T}}\|}, \tag{23}$$

or, in component form,

$$v^{\alpha}_{\mathrm{T}} = \zeta m^{\alpha\beta} t_{\mathrm{T}_\beta} [t_{\mathrm{T}_\gamma} m^{\gamma\rho} t_{\mathrm{T}_\rho}]^{-1/2}. \tag{24}$$

Manipulation of (24) reveals an alternate form that defines ζ as a (notably non-negative) norm of the slip velocity. Evolution of tangential motion and forces is thus governed by the following stick/slip conditions (in component form)

$$\begin{aligned} &\Phi := [t_{\mathrm{T}_\alpha} m^{\alpha\beta} t_{\mathrm{T}_\beta}]^{1/2} - \mu t_{\mathrm{N}} \leqslant 0, \\ &\zeta := [v^{\alpha}_{\mathrm{T}} m_{\alpha\beta} v^{\beta}_{\mathrm{T}}]^{1/2} \geqslant 0, \\ &\Phi\zeta = 0. \end{aligned} \tag{25}$$

The *stick parameter* Φ in $(25)_1$ is defined so as to maximize the tangential force at a constant coefficient of friction multiple μ of the normal force t_{N}. The consistency condition $(25)_3$ ensures that negative Φ are associated with zero tangential motion, or 'stick' friction, while positive values of ζ, indicative of 'slip' motion between the contact surfaces, corresponds with a maximum application of tangential surface force $\|\boldsymbol{t}_{\mathrm{T}}\| = \mu t_{\mathrm{N}}$.

2.4. Conservation and consistent dissipation

Under the current presumptions of free (unforced) motion, the continuum system (7) adheres to a set of physically motivated balance laws, including the global balance of linear momentum, $\boldsymbol{L}_t$, and of angular momentum, $\boldsymbol{J}_t$, each related to the state of the system by definitions

$$\boldsymbol{L}_t := \sum_i^2 \int_{\Omega^{(i)}} \rho_0^{(i)} \boldsymbol{V}_t^{(i)} \, \mathrm{d}\Omega^{(i)} \tag{26}$$

and

$$\boldsymbol{J}_t := \sum_i^2 \int_{\Omega^{(i)}} \rho_0^{(i)} \boldsymbol{\varphi}_t^{(i)} \times \boldsymbol{V}_t^{(i)} \, \mathrm{d}\Omega^{(i)}. \tag{27}$$

Thermodynamic consistency for an unforced system requires that total system energy, E_t^{tot}, either remain constant or decrease. We expect the former for elastic bulk descriptions (by definition) and for frictionless contact phenomena, and the latter for physically dissipative inelastic bulk descriptions and frictional contact. Total system energy is defined as a sum of kinetic (K_t) and internal (E_t^{int}) energies,

$$E_t^{\mathrm{tot}} = K_t + E_t^{\mathrm{int}}, \tag{28}$$

with kinetic energy arising from the material velocities such that

$$K_t := \frac{1}{2} \sum_i^2 \langle \rho_0 \boldsymbol{V}_t, \boldsymbol{V}_t \rangle^{(i)} \tag{29}$$

and where the time derivative of the internal energy can be expressed in terms of an *internal dissipation function*, $\mathscr{D}_t^{\mathrm{int}} \geqslant 0$, and an integral-valued *internal stress power*, $\mathscr{P}_t^{\mathrm{int}}$:

$$\frac{\mathrm{d}E_t^{\mathrm{int}}}{\mathrm{d}t} = \mathscr{P}_t^{\mathrm{int}} - \mathscr{D}_t^{\mathrm{int}} = \sum_i^2 \langle D\boldsymbol{\varphi}_t \boldsymbol{S}_t, \mathrm{GRAD}[\boldsymbol{V}_t] \rangle^{(i)} - \mathscr{D}_t^{\mathrm{int}}. \tag{30}$$

We continue development by precluding internal dissipation, ($\mathscr{D}_t^{\text{int}} = 0$), and make suitable substitutions for the variations $\overset{*}{\boldsymbol{\varphi}}$ into the variational equation (7) to demonstrate that the continuum system, subject to the constraints (22) and (25), will completely conserve both linear and angular momenta, and will exhibit a quantifiable contact-associated energy dissipation $\mathscr{D}_t^{\text{c}}$ according to the equation

$$\frac{\mathrm{d}E_t^{\text{tot}}}{\mathrm{d}t} = -\mathscr{D}_t^{\text{c}} = -\int_{\Gamma_{\text{c}}} (\mu t_{\text{N}} \zeta)\, \mathrm{d}\Gamma_{\text{c}} \leqslant 0. \tag{31}$$

The energy dissipation in (31) requires the evolution of frictional slip, and will be zero for stick friction ($\zeta = 0$) or in the absence of friction ($\mu = 0$).

Our goal in the subsequent algorithmic development is to preserve not only the conservative characteristics of the bulk continuum and normal contact constraints, but to also suitably approximate the frictional dissipation as both dissipative and proportional to the localized slip motion and tangential contact forces, as suggested by the continuum estimate in (31).

3. Algorithmic development

The following is a frictional extension of the frictionless algorithmic development in Laursen and Love [11], and similarly presumes direct application of the conservation arguments for non-linear elastodynamic continuua as constructed by Simo and Tarnow [16]. In the development we are careful to use objective descriptions of the discrete tangential variations and discrete tangential motions on the fashion of Armero and Petocz [2], thus ensuring conservation of angular momentum in the force vectors as well as in the discrete velocity updates which are constructed from an analogous framework.

3.1. System discretization within an energy–momentum framework

To establish a suitable framework for a spatial finite element discretization we once again consider the variational form of the momentum equation (2). In standard fashion we introduce finite dimensional approximations for the deformation ($\boldsymbol{\varphi}_t^h$), and the variation ($\overset{*}{\boldsymbol{\varphi}}{}^h$), within the appropriate discrete functional spaces so that

$$\boldsymbol{\varphi}_t^h = \sum_{A=1}^{n_{\text{nod}}} N_A \boldsymbol{d}_A(t) \tag{32}$$

and

$$\overset{*}{\boldsymbol{\varphi}}{}^h = \sum_{A=1}^{n_{\text{nod}}} N_A \overset{*}{\boldsymbol{d}}_A. \tag{33}$$

The displacement vector $\boldsymbol{d}_A(t)$ and variational vector $\overset{*}{\boldsymbol{d}}_A$ contain values for each of the n_{sd} spatial dimensions and correspond with a nodally discrete local vector value indexed by $A = \{1, \ldots, n_{\text{nod}}\}$. Discrete material velocity values follow the description $\boldsymbol{v}_A(t) = \dot{\boldsymbol{d}}_A(t)$ and can be used as approximations to their continuum counterparts through suitable weighting by finite element shape functions N_A, each of which is expressed over the domain $\overline{\Omega}^{(1)} \cup \overline{\Omega}^{(2)}$. We will maintain a notation that designates *unindexed* state vectors ($\boldsymbol{d}(t)$, $\overset{*}{\boldsymbol{d}}$ and $\boldsymbol{v}(t)$) as global compilations of their respective state values over all nodes and for each spatial dimension, giving each a total vector length corresponding to the number of nodal equations ($n_{\text{neq}} = n_{\text{sd}} \cdot n_{\text{nod}}$).

We adopt in large part a traditional notation for temporal discretization, first subdividing the time period $\mathbb{I}$ into discrete n-indexed *time steps* $[t_n, t_{n+1}]$, and denoting the length of each increment with

$\Delta t = t_{n+1} - t_n$. Approximations of "endpoint" state values corresponding with these particular time points are similarly indexed, such that $\boldsymbol{d}_n \approx \boldsymbol{d}(t_n)$, $\boldsymbol{v}_n \approx \boldsymbol{v}(t_n)$. etc. Intermediate points in time are then described with the aid of a single parameter, $\alpha \in [0,1]$, such that $t_{n+\alpha} = t_n + \alpha\Delta t$, and intermediate state values can be approximated through a similar *convex combination* of the endpoint values, e.g.

$$\boldsymbol{d}_{n+\alpha} = \alpha\boldsymbol{d}_{n+1} + (1-\alpha)\boldsymbol{d}_n, \quad \alpha \in [0,1]. \tag{34}$$

In anticipation of a conservative structure, we use subscript brackets to denote a state that is associated with an intermediate configuration and/or time but for which a convex combination approximation is not suitable, as in the example of a general and fully discrete description of the stress tensor, $\boldsymbol{S}_{[n+\alpha]}$, where

$$\boldsymbol{S}_{[n+\alpha]} \approx \boldsymbol{S}(\boldsymbol{d}(t_{n+\alpha})) \neq \alpha\boldsymbol{S}_{n+1} + (1-\alpha)\boldsymbol{S}_n. \tag{35}$$

A truncated Taylor's series expansion in time completes the temporal discretization with a suitable approximation for time derivatives of the state variables:

$$\begin{aligned} \boldsymbol{v}_{n+1/2} &\approx (\dot{\boldsymbol{d}})_{n+1/2} = \frac{1}{\Delta t}[\boldsymbol{d}_{n+1} - \boldsymbol{d}_n] + \mathrm{O}(\Delta t^2), \\ (\dot{\boldsymbol{v}})_{n+1/2} &= \frac{1}{\Delta t}[\boldsymbol{v}_{n+1} - \boldsymbol{v}_n] + \mathrm{O}(\Delta t^2). \end{aligned} \tag{36}$$

Given (32)–(36), and adopting a midpoint equilibrium configuration $\alpha = 1/2$, we consider a full discretization of the internal virtual work expression (4) as

$$G^h(\boldsymbol{d}_{n+1/2}, \overset{*}{\boldsymbol{d}}) = \sum_{A=1}^{n_{\mathrm{nod}}} \sum_{B=1}^{n_{\mathrm{nod}}} \left[\frac{1}{\Delta t} M_{AB}[\boldsymbol{v}_{n+1_B} - \boldsymbol{v}_{n_B}] + \boldsymbol{f}^{\mathrm{int}}_{[n+1/2]_A} \right] \cdot \overset{*}{\boldsymbol{d}}_A. \tag{37}$$

The nodal mass contributions M_{AB} in (37) assume a standard form

$$M_{AB} = \langle \rho_0 N_A, N_B \rangle, \tag{38}$$

and the nodal internal forces $\boldsymbol{f}^{\mathrm{int}}_A$ are given by

$$\boldsymbol{f}^{\mathrm{int}}_{[n+1/2]_A} = \sum_{B=1}^{n_{\mathrm{nod}}} \left\langle \mathrm{GRAD}[N_B]\boldsymbol{d}^T_{n+1/2_B}\boldsymbol{S}_{[n+1/2]}, \mathrm{GRAD}[N_A] \right\rangle. \tag{39}$$

$\boldsymbol{S}_{[n+1/2]}$ represents an algorithmic form of the internal stresses as subject to an obstensibly midpoint-oriented discretization of the constitutive relationship. We presume a suitable discretization such that this approximation of the second Piola–Kirchhoff stress is conservative and second order accurate in time according to the elastodynamic developments of Simo and Tarnow [16] and Gonzalez [8].

3.2. Contact surface discretization

Adopting a midpoint configuration, we similarly discretize the contact virtual work expression (6) according to the expression

$$G^h_{\mathrm{c}}(\boldsymbol{d}_{n+1/2}, \overset{*}{\boldsymbol{d}}) = -\sum_{A=1}^{n_{\mathrm{nod}}} \boldsymbol{f}^{\mathrm{c}}_{[n+1/2]_A} \cdot \overset{*}{\boldsymbol{d}}_A, \tag{40}$$

which we describe using a set of definitions synonymous to those in Laursen and Simo [12], constructing the nodal contact forces $\boldsymbol{f}^{\mathrm{c}}_A$ from an integration of discrete normal ($\boldsymbol{N}_A$), and dilitational/tangential ($\boldsymbol{D}^{\alpha}_A$) contributions of the tractions on the contact surface,

$$\boldsymbol{f}^{\mathrm{c}}_{[n+1/2]_A} = \int_{\Gamma_{\mathrm{c}}} \left(t_{\mathrm{N}}\boldsymbol{N}_{[n+1/2]_A} - t_{\mathrm{T}_\alpha}\boldsymbol{D}^{\alpha}_{[n+1/2]_A} \right) \mathrm{d}\Gamma_{\mathrm{c}}. \tag{41}$$

To complete the discretization we can evaluate the contact integral with a set of n_{int} contact quadrature points $\boldsymbol{X}^l \in \Gamma_{\text{c}}^{(1)}$, and denote associated evaluations with a similar superscript. We then construct the nodal contact forces as a sum of the quadrature point contributions, representing a weight of integration for each quadrature point with w^l and resolving the parameter transformation with a quadrature Jacobean representation j^l. Summing over all quadrature points yields a fully discrete description for the nodal contact forces

$$\boldsymbol{f}^{\text{c}}_{[n+1/2]_A} = \sum_{l=1}^{n_{\text{int}}} w^l j^l \left[t^l_{\text{N}} \boldsymbol{N}^l_{[n+1/2]_A} - t^l_{\text{T}_\alpha} \boldsymbol{D}^{\alpha l}_{[n+1/2]_A} \right]. \tag{42}$$

The directional contributions are in turn defined pointwise in terms of the surface geometry (normal and tangential vectors $\boldsymbol{v}$ and $\boldsymbol{\tau}$ as well as gap function g) through a nodal *projection operator*, P_A:

$$\begin{aligned} &\boldsymbol{N}_A := P_A \boldsymbol{v}, \\ &\boldsymbol{T}_{\alpha A} := P_A \boldsymbol{\tau}_\alpha, \\ &A_{\alpha\beta} \boldsymbol{D}^\alpha_A := \boldsymbol{T}_{\beta A} + g \boldsymbol{N}_{A,\beta}, \\ &A_{\alpha\beta} := m_{\alpha\beta} + (g \boldsymbol{v} \cdot \boldsymbol{\tau}_{\alpha,\beta}). \end{aligned} \tag{43}$$

The projection operator, as described in Laursen and Love [11], is defined over all nodes in the mesh (n_{nod}), but potentially non-zero only for nodes associated with the contact surface. The specific definition of the operator and of its spatial derivative on the contact surface both depend upon the body associated with the given node A and essentially maintain the equal and opposite nature of the contact surface forces. For nodes A on $\Gamma_{\text{c}}^{(1)}$ we define

$$P_A = N_A(\boldsymbol{X}) \quad \text{and} \quad P_{A,\beta} = 0. \tag{44}$$

Points $\boldsymbol{X}$ on $\Gamma_{\text{c}}^{(1)}$ are independent of the contact projection parameter associated with the index β and thus the spatial derivative is zero. For nodes A on $\Gamma_{\text{c}}^{(2)}$ we define

$$P_A = -N_A(\overline{\boldsymbol{Y}}(\boldsymbol{X}, t)) \quad \text{and} \quad P_{A,\beta} = -N_{A,\beta}(\overline{\boldsymbol{Y}}(\boldsymbol{X}, t)). \tag{45}$$

The projection operator also provides a means of discretizing the kinematic surface variables in terms of nodal displacements. From the descriptions in Section 2.2, we establish discrete descriptions of the surface normal and tangential basis

$$\boldsymbol{v} = -\frac{1}{|\, g \,|} \sum_{A=1}^{n_{\text{nod}}} P_A \boldsymbol{d}_A, \tag{46}$$

$$\boldsymbol{\tau}_\alpha = -\sum_{A=1}^{n_{\text{nod}}} P_{A,\alpha} \boldsymbol{d}_A, \tag{47}$$

which in turn require a definition for the magnitude of the gap function

$$|\, g \,| = \left[\sum_{A=1}^{n_{\text{nod}}} \sum_{B=1}^{n_{\text{nod}}} P_A P_B \boldsymbol{d}_A \cdot \boldsymbol{d}_B \right]^{1/2}. \tag{48}$$

Gap and slip variations are simply derived through use of nodal variations, $\overset{*}{\boldsymbol{d}}_A$,

$$\delta g = -\boldsymbol{v} \cdot \sum_{A=1}^{n_{\text{nod}}} P_A \overset{*}{\boldsymbol{d}}_A = -\sum_{A=1}^{n_{\text{nod}}} \boldsymbol{N}_A \cdot \overset{*}{\boldsymbol{d}}_A, \tag{49}$$

$$\delta \bar{\xi}^\alpha = A^{\alpha\beta} \left(\boldsymbol{\tau}_\beta \cdot \sum_{A=1}^{n_{\text{nod}}} P_A \overset{*}{\boldsymbol{d}}_A + g \boldsymbol{v} \cdot \sum_{A=1}^{n_{\text{nod}}} P_{A,\beta} \overset{*}{\boldsymbol{d}}_A \right) = \sum_{A=1}^{n_{\text{nod}}} \boldsymbol{D}^\alpha_A \cdot \overset{*}{\boldsymbol{d}}_A, \tag{50}$$

which applies similarly for the gap and slip rates using nodal velocities:

$$v_{\mathrm{N}} = -\sum_{A=1}^{n_{\mathrm{nod}}} \boldsymbol{N}_A \cdot \boldsymbol{v}_A, \tag{51}$$

$$\boldsymbol{v}_{\mathrm{T}}^{\alpha} = \sum_{A=1}^{n_{\mathrm{nod}}} \boldsymbol{D}_A^{\alpha} \cdot \boldsymbol{v}_A. \tag{52}$$

The description (41) and (43) thus yields a direct discretization of the contact virtual work, leaving the magnitudes of the discrete contact surface forces t_{N} and t_{T_α} as variables to be determined by local algorithmic enforcement of the contact constraints:

$$G_{\mathrm{c}}^{h}(\boldsymbol{d}_{n+1/2}, \overset{*}{\boldsymbol{d}}) = -\sum_{A=1}^{n_{\mathrm{nod}}} \boldsymbol{f}^{\mathrm{c}}_{[n+1/2]_A} \cdot \overset{*}{\boldsymbol{d}}_A = \sum_{l=1}^{n_{\mathrm{int}}} \left[t^l_{\mathrm{N}}\, \delta g^l_{[n+1/2]} + t^l_{\mathrm{T}_\alpha}\, \delta \bar{\xi}^{\alpha l}_{[n+1/2]} \right]. \tag{53}$$

3.3. The velocity-update form

Whereas the temporal approximation for the velocity in $(36)_1$ is derived from a system with presumedly continuous derivatives, we note, as in Laursen and Love [11], that solid impacts are generally characterized by instantaneous changes in velocity at the contact surface, as warranted by the persistency condition $(22)_4$. As in the previous manuscript, we consequently append a *discrete contact velocity*, $\boldsymbol{v}^{\mathrm{c}}$, to the velocity/displacement relationship in the equations of motion in order to represent these effects. Consider first the variational momentum equation, fully discretized and expressed in *displacement form*, i.e. in terms of endpoint displacements ($\boldsymbol{d}_{n+1}$) but excluding endpoint velocities ($\boldsymbol{v}_{n+1}$):

$$G^{h}(\boldsymbol{d}_{n+1/2}, \overset{*}{\boldsymbol{d}}) + G_{\mathrm{c}}^{h}(\boldsymbol{d}_{n+1/2}, \overset{*}{\boldsymbol{d}}) = \sum_{A=1}^{n_{\mathrm{nod}}} \sum_{B=1}^{n_{\mathrm{nod}}} \left[\frac{2}{\Delta t} M_{AB} \left[-\boldsymbol{v}_{n_B} + \frac{1}{\Delta t} \Delta \boldsymbol{d}_B \right] + \boldsymbol{f}^{\mathrm{int}}_{[n+1/2]_A} + \boldsymbol{f}^{\mathrm{c}}_{[n+1/2]_A} \right] \cdot \overset{*}{\boldsymbol{d}}_A = 0. \tag{54}$$

In this form, the momentum equations can be solved in terms of the displacement increment, $\Delta \boldsymbol{d} = \boldsymbol{d}_{n+1} - \boldsymbol{d}_n$. We address the inclusion of the discrete contact velocities *after* convergence of the displacements, suitably adjusting the post-contact velocities $\boldsymbol{v}_{n+1}$ according to the formula

$$\boldsymbol{v}_{n+1_A} = -\boldsymbol{v}_{n_A} + \frac{2}{\Delta t} \Delta \boldsymbol{d}_A + \boldsymbol{v}^{\mathrm{c}}_A. \tag{55}$$

In a spatially discrete system, a temporally discrete velocity jump must be represented nodally and thus correlates to a jump in momentum as weighted by the contributing nodal masses. As in the frictionless case, we require the that the momentum changes induced by these contact velocities assume the same balanced form as the discrete contact forces, with the notable selection of the endstate $(n+1)$ configuration and not the midpoint $(n+1/2)$ configuration. We further presume that the relative magnitudes of the normal and tangential contributions remain consistent with the local contact force magnitudes at the quadrature points, and thus we can represent the magnitude of the change as a multiple of the contact force terms through a local variable κ:

$$\sum_{B=1}^{n_{\mathrm{nod}}} M_{AB} \boldsymbol{v}^{\mathrm{c}}_B = \sum_{l=1}^{n_{\mathrm{int}}} w^l j^l \kappa^l \left[t^l_{\mathrm{N}} \boldsymbol{N}^l_{[n+1]_A} - t^l_{\mathrm{T}_\alpha} \boldsymbol{D}^{\alpha l}_{[n+1]_A} \right]. \tag{56}$$

The effect of this term essentially mimics the initiation of an impact induced stress/velocity wavefront and the initial stages of wave propagation. We note that through the prescription in (56), these effects are

described in the discrete system based on the local nodal geometry of the contact surface designated by the projection shape functions P_A within the definitions of $\boldsymbol{N}_A$ and $\boldsymbol{D}_A^{\alpha}$. Note however, that velocity update effects will not remain local, but will be propagated through the bulk media over the course of a single time step, given the coupling of internal and contact surface nodes through the mass matrix M_{AB}. The common practice of using a lumped mass matrix (as in the examples of this manuscript) serves to eliminate the nodal coupling to thus localize the internal velocity updates, and it also simplifies the extraction of the contact update values from (56) by trivializing the inversion of M_{AB}. For relatively low material wavespeeds and/or small time steps actual wave effects themselves will indeed be limited to the vicinity of the contact surface during a given time step; however as wave speeds grow large, particularly in the rigid body limit, the physical wavespeed effects are likely to be systemic even within a single step, and can only be suitably distributed algorithmically using a consistent mass matrix. Therefore we note that the algorithmic convenience of a lumped mass matrix may only be conditionally suitable for velocity-update calculations.

We also note that the κ values in (56) can be related directly to the impulse magnitudes p in the notation of the frictionless development [11] through the contact force terms, where $p_{\mathrm{N}} = \kappa t_{\mathrm{N}}$.

3.4. Momentum conservation

In Laursen and Love [11] the discrete contact velocity term provides additional and necessary latitude for the enforcement of the normal contact constraints under the stricter confines of energy conservation. We wish to adhere to nearly the same requirements for the tangential constraints, enforcing conservation conditions locally for stick friction and allowing dissipation consistent with the continuum solution for slip friction. The conditions can be generated as in the previous manuscript, by considering a sequence of variational substitutions into the fully discretized local equations, (54) and (55), and presuming the use of a conserving methodology in the determination of the internal force vector $\boldsymbol{f}^{\mathrm{int}}$ such that the internal term generates a change in internal potential for the energy argument and vanishes for the momentum arguments. The momentum discussion is relatively straightforward.

For example, presuming *arbitrary translations*, $\overset{*}{\boldsymbol{d}}_A = \boldsymbol{\eta}$, ($\boldsymbol{\eta}$ spatially constant), the discrete system (54) can be shown to demonstrate conservation of linear momentum when

$$\boldsymbol{L}_{n+1} - \boldsymbol{L}_n := \sum_{A=1}^{n_{\mathrm{nod}}} \left[\sum_{B=1}^{n_{\mathrm{nod}}} M_{AB} \boldsymbol{v}_B^{\mathrm{c}} + \Delta t \boldsymbol{f}^{\mathrm{c}}_{[n+1/2]_A} \right] = \boldsymbol{0}. \tag{57}$$

Similarly, presuming *arbitrary rotations*, $\overset{*}{\boldsymbol{d}}_A = \boldsymbol{\eta} \times \boldsymbol{d}_{n+1/2_A}$, ($\boldsymbol{\eta}$ spatially constant), the discrete system can be shown to demonstrate conservation of angular momentum when

$$\boldsymbol{J}_{n+1} - \boldsymbol{J}_n := \sum_{A=1}^{n_{\mathrm{nod}}} \left[\sum_{B=1}^{n_{\mathrm{nod}}} M_{AB} (\boldsymbol{d}_{n+1_A} \times \boldsymbol{v}_B^{\mathrm{c}}) + \Delta t \left(\boldsymbol{d}_{n+1/2_A} \times \boldsymbol{f}^{\mathrm{c}}_{[n+1/2]_A} \right) \right] = \boldsymbol{0}. \tag{58}$$

From conditions (57) and (58) it is apparent that the discrete structure of both the contact force vector and the velocity update are crucial to enforcement of the momentum conservation conditions. In both cases the discrete definitions ((42) and (56)) inherit the 'equal and opposite' nature of contact in the continuum through the definition of the projection operator in (44) and (45). For *each* quadrature point on the shared contact surface, equally weighted contributions from nodes on both contacting bodies will cancel, i.e. for a generic configuration,

$$\sum_{A=1}^{n_{\mathrm{nod}}} \boldsymbol{N}^{I}_{[n+\gamma]_A} = \boldsymbol{0} \tag{59}$$

and

$$\sum_{A=1}^{n_{\text{nod}}} \boldsymbol{D}^{\alpha l}_{[n+\gamma]_A} = \boldsymbol{0}. \tag{60}$$

By definitions (41) and (56) we then find that over all points in the contact surface,

$$\sum_{A=1}^{n_{\text{nod}}} \boldsymbol{f}^{\text{c}}_{[n+1/2]_A} = \boldsymbol{0} \tag{61}$$

and

$$\sum_{A=1}^{n_{\text{nod}}} \sum_{B=1}^{n_{\text{nod}}} M_{AB} \boldsymbol{v}_{\text{c}} = \boldsymbol{0}, \tag{62}$$

effectively establishing the condition for linear momentum conservation (57) independent of the contact force and velocity update magnitudes. The angular momentum conditions must be handled more carefully. Consider first the cross product summation over the contact forces,

$$\sum_{A=1}^{n_{\text{nod}}} \boldsymbol{d}_{n+1/2_A} \times \boldsymbol{f}^{\text{c}}_{A[n+1/2]} = -\sum_{A=1}^{n_{\text{nod}}} \sum_{l=1}^{n_{\text{int}}} w^l j^l \left[t^l_{\text{N}} \boldsymbol{N}^l_{[n+1/2]_A} \times \boldsymbol{d}_{n+1/2_A} - t^l_{\text{T}_\alpha} \boldsymbol{D}^{\alpha l}_{[n+1/2]_A} \times \boldsymbol{d}_{n+1/2_A} \right]. \tag{63}$$

Expanding $\boldsymbol{N}$ according to the definition $(43)_1$ and taking advantage of the discrete surface normal description (46) yields

$$\begin{aligned} \sum_{A=1}^{n_{\text{nod}}} \boldsymbol{N}_{[n+1/2]_A} \times \boldsymbol{d}_{n+1/2_A} &= \sum_{A=1}^{n_{\text{nod}}} P_{[n+1/2]_A} \boldsymbol{v}_{[n+1/2]} \times \boldsymbol{d}_{n+1/2_A} \\ &= \boldsymbol{v}_{[n+1/2]} \times \left(\sum_{A=1}^{n_{\text{nod}}} P_{[n+1/2]_A} \boldsymbol{d}_{n+1/2_A} \right) \\ &= \boldsymbol{v}_{[n+1/2]} \times \left(- g_{[n+1/2]} \boldsymbol{v}_{[n+1/2]} \right) = \boldsymbol{0}, \end{aligned} \tag{64}$$

whereas expanding the components of $\boldsymbol{D}^\alpha$ from the definitions in (43) and the tangent description (47) yields terms that cancel locally, namely

$$\begin{aligned} \sum_{A=1}^{n_{\text{nod}}} \boldsymbol{T}_{\beta[n+1/2]_A} \times \boldsymbol{d}_{n+1/2_A} &= \sum_{A=1}^{n_{\text{nod}}} P_{[n+1/2]_A} \boldsymbol{\tau}_{\beta[n+1/2]} \times \boldsymbol{d}_{n+1/2_A} \\ &= \boldsymbol{\tau}_{\beta[n+1/2]} \times \left(\sum_{A=1}^{n_{\text{nod}}} P_{[n+1/2]_A} \boldsymbol{d}_{n+1/2_A} \right) \\ &= \boldsymbol{\tau}_{\beta[n+1/2]} \times \left(- g_{[n+1/2]} \boldsymbol{v}_{[n+1/2]} \right) \end{aligned} \tag{65}$$

and

$$\begin{aligned} g_{[n+1/2]} \sum_{A=1}^{n_{\text{nod}}} \boldsymbol{N}_{[n+1/2]_{A,\beta}} \times \boldsymbol{d}_{n+1/2_A} &= g_{[n+1/2]} \sum_{A=1}^{n_{\text{nod}}} P_{[n+1/2]_{A,\beta}} \boldsymbol{v}_{[n+1/2]} \times \boldsymbol{d}_{n+1/2_A} \\ &= g_{[n+1/2]} \boldsymbol{v}_{[n+1/2]} \times \left(\sum_{A=1}^{n_{\text{nod}}} P_{[n+1/2]_{A,\beta}} \boldsymbol{d}_{n+1/2_A} \right) \\ &= g_{[n+1/2]} \boldsymbol{v}_{[n+1/2]} \times \left(- \boldsymbol{\tau}_{\beta[n+1/2]} \right) = \boldsymbol{\tau}_{\beta[n+1/2]} \times g_{[n+1/2]} \boldsymbol{v}_{[n+1/2]}. \end{aligned} \tag{66}$$

This convenient result is a direct consequence of adopting the dilitational form (15) for the tangential contact force, despite the apparent redundancy of the latter term (given that in contact, $g = 0$ in the continuum form).

We see a similar set of results for the velocity update contributions,

$$\sum_{A=1}^{n_{\text{nod}}}\sum_{B=1}^{n_{\text{nod}}} M_{AB}\boldsymbol{d}_{n+1_A}\times\boldsymbol{v}^{\text{c}}_B = -\sum_{A=1}^{n_{\text{nod}}}\sum_{l=1}^{n_{\text{int}}} w^l j^l \kappa^l \left[t^l_{\text{N}}\boldsymbol{N}^l_{[n+1]_A}\times\boldsymbol{d}_{n+1_A} - t^l_{\text{T}_\alpha}\boldsymbol{D}^{\alpha l}_{[n+1]_A}\times\boldsymbol{d}_{n+1_A}\right], \tag{67}$$

and note that the arguments proceed similarly, with an obvious contingency on the $n+1$ configuration. As in the case of linear momentum, angular momentum is again conserved independent both of the contact forces and of the choice of relative velocity update values κ^l, and thus

$$\boldsymbol{J}_{n+1} - \boldsymbol{J}_n = \boldsymbol{0}. \tag{68}$$

3.5. Ensuring energy consistency

To establish an algorithmic system that is consistent with physical expectations, we must establish fully discrete a priori estimates of contact dissipation. The total dissipation can be considered as a sum of local quadrature point contributions,

$$\mathscr{D}^{\text{c}}_{[n+1/2]} = \sum_{l=1}^{n_{\text{int}}} \mathscr{D}^{\text{c}^l}_{[n+1/2]}. \tag{69}$$

For stick friction at a quadrature point, we expect no local dissipation, i.e.

$$\text{STICK}:\ \mathscr{D}^{\text{c}^l}_{[n+1/2]} = 0, \tag{70}$$

while for slip friction, we establish our estimate with a midpoint discretization of continuum estimate (31), so that

$$\text{SLIP}:\ \mathscr{D}^{\text{c}^l}_{[n+1/2]} = \left(\mu t_{\text{N}}\zeta_{[n+1/2]}\right)^l. \tag{71}$$

Then we return again to the momentum equation (54) and choose the set of *local displacement increments*, $\overset{*}{\boldsymbol{d}}_A = \Delta\boldsymbol{d}_A$ as variations. Substituting velocity values where appropriate through (55) and presuming a conserving integration of the internal energy, we can quantify the actual *algorithmic* energy loss as a function of the contact force and discrete contact velocity vectors, such that

$$E^{\text{tot}}_{n+1} - E^{\text{tot}}_n := \sum_{A=1}^{n_{\text{nod}}}\left[\sum_{B=1}^{n_{\text{nod}}} M_{AB}\left(\frac{2}{\Delta t}\Delta\boldsymbol{d}_B - \boldsymbol{v}_{n_B} + \frac{1}{2}\boldsymbol{v}^{\text{c}}_B\right)\cdot\boldsymbol{v}^{\text{c}}_A + \Delta\boldsymbol{d}_A\cdot\boldsymbol{f}^{\text{c}}_{[n+1/2]_A}\right]. \tag{72}$$

We would like to ensure that this algorithmic energy loss directly represents the estimated contact dissipation over a time step, so that

$$E^{\text{tot}}_{n+1} - E^{\text{tot}}_n = -\Delta t\mathscr{D}^{\text{c}}_{[n+1/2]}. \tag{73}$$

The energy balance condition (73) contains a useful set of unknowns, namely the local magnitudes, κ^l, that define the contact velocity terms, $\boldsymbol{v}^{\text{c}}$. To extract these values, we resolve definition (72) into vector components using a second quadrature summation (indexed k) as well as a matrix inversion of the mass term. As in the frictionless case we simplify notation by introducing quadratic coefficients (A^{kl}, b^l, c^l, with no sum implied on quadrature point indices k and l):

$$\begin{aligned}
A^{kl} &:= \frac{1}{2}\sum_{A=1}^{n_{\text{nod}}}\sum_{B=1}^{n_{\text{nod}}} w^l w^k j^l j^k M^{-1}_{AB}\left[t^l_{\text{N}}\boldsymbol{N}^l_{[n+1]_A} - t^l_{\text{T}_\alpha}\boldsymbol{D}^{\alpha l}_{[n+1]_A}\right]\cdot\left[t^k_{\text{N}}\boldsymbol{N}^k_{[n+1]_B} - t^k_{\text{T}_\beta}\boldsymbol{D}^{\beta k}_{[n+1]_B}\right],\\
b^l &:= \sum_{A=1}^{n_{\text{nod}}} w^l j^l\left(\frac{2}{\Delta t}\Delta\boldsymbol{d}_A - \boldsymbol{v}_{n_A}\right)\cdot\left[t^l_{\text{N}}\boldsymbol{N}^l_{[n+1]_A} - t^l_{\text{T}_\alpha}\boldsymbol{D}^{\alpha l}_{[n+1]_A}\right],\\
c^l &:= \Delta t w^l j^l\mathscr{D}^{\text{c}^l}_{[n+1/2]} + \sum_{A=1}^{n_{\text{nod}}} w^l j^l\left[t^l_{\text{N}}\boldsymbol{N}^l_{[n+1/2]_A} - t^l_{\text{T}_\alpha}\boldsymbol{D}^{\alpha l}_{[n+1/2]_A}\right]\cdot\Delta\boldsymbol{d}_A.
\end{aligned} \tag{74}$$

Values κ^l can then be chosen to satisfy the coupled quadratic equations

$$\sum_{l=1}^{n_{\text{int}}} \left[\sum_{k=1}^{n_{\text{int}}} (A^{kl}\kappa^k\kappa^l) + b^l\kappa^l + c^l \right] = 0, \tag{75}$$

constructing the velocity update $\boldsymbol{v}^{\text{c}}$ in (55) so that the unintended algorithmic dissipation has been, in essence, 'returned' to the discrete system as a modification to the kinetic energy. Local enforcement of (75) at each quadrature point l succumbs easily to linearization and thus to solution by a Newton–Raphson or similar iterative solver, using the same solution selection criteria as in the frictionless case [11]. As in that case, however, solutions are only guaranteed to exist under the provision that the system without the velocity update (where $\kappa^l = 0$) is overly dissipative, i.e. when

$$c^l \leqslant 0. \tag{76}$$

Our notation will presume that time-discrete gap and slip rates that are independent of the contact velocity updates, thus coefficients c^l are more simply written using definitions (50) and (52) for stick and slip cases coinciding with (70) and (71) respectively:

$$\text{STICK:}\;\; c^l = -\Delta t w^l j^l \left(t_{\text{N}} v_{\text{N}_{[n+1/2]}} + t_{\text{T}_\alpha} v^\alpha_{\text{T}_{[n+1/2]}} \right)^l, \tag{77}$$

$$\text{SLIP:}\;\; c^l = -\Delta t w^l j^l \left(t_{\text{N}} v_{\text{N}_{[n+1/2]}} + t_{\text{T}_\alpha} v^\alpha_{\text{T}_{[n+1/2]}} - \mu t_{\text{N}} \zeta_{[n+1/2]} \right)^l. \tag{78}$$

3.6. Discrete constraint enforcement

The evolution of the contact force magnitude terms (t_{N} and t_{T_α}) is governed by respective sets of contact constraints (22) and (25) which in the continuum case prevent interpenetration of the two bodies while simultaneously ensuring conservation of energy for frictionless constraints and consistent dissipation in the presence of friction. Discretization of the system, however, introduces a potential discrepancy in achieving the combined goals of local constraint enforcement and global energy conservation, as encountered in the considerations of frictionless dynamic impact by both Armero and Petocz [1] and Laursen and Chawla [10].

The contact velocity term alleviates this discrepancy, allowing for full enforcement of the contact conditions for each algorithmic state, within the limits of an algorithmic regularization. Consider, for example, an augmented Lagrangian formulation for frictional contact (see [15]). We can adopt the normal constraints directly from the frictionless case, expressing normal force t_{N} as a function of a penalty value $\boldsymbol{\epsilon}_{\text{N}}$ and positive portions of the the gap function (as selected by the MacAulay bracket $\langle\cdot\rangle$), as well as a *fixed* multiplier iterate $\lambda_{\text{N}}^{(k)}$:

$$t_{\text{N}} = \langle \lambda_{\text{N}}^{(k)} + \boldsymbol{\epsilon}_{\text{N}} (g_{n+1} - \langle g_n \rangle) \rangle. \tag{79}$$

This regularization will reproduce the impenetrability condition $(22)_3$ at the end-step (time t_{n+1}) for newly initiated contact but reverts to an enforcement of the persistency condition $(22)_4$ for continued contact. We note that this strategy of enforcing an initial endstep constraint ($g_{n+1} \leqslant 0$) and then enforcing a zero rate of change in the constraint for subsequent steps is equivalent (in the regularization limit) to a repeated direct enforcement of the constraint, albeit more heavily prone to errors generated by incomplete enforcement of the constraint in the first step. The benefit, however, is that the normal contact force is consequently always positive by definition, and is only applied when the mid-point gap rate is also positive ($v_{\text{N}_{[n+1/2]}} > 0$), thus assuring that the normal contribution to the contact dissipation in (77) and (78) is of the appropriate sign,

Table 1
Summary of contact conditions

Gap conditions	Description	Normal contact force, t_N
$g_n < 0,\ g_{n+1} < 0$	Out of contact	0
$g_n < 0,\ g_{n+1} \geqslant 0$	New contact	$\lambda_N + \epsilon_N g_{n+1} \geqslant 0$
$g_n \geqslant 0,\ g_{n+1} < 0$	Complete release	0
$0 \leqslant g_n \leqslant g_{n+1}$	Persistent contact	$\lambda_N + \epsilon_N \Delta t v_{N[n+1/2]} \geqslant 0$
$0 < g_{n+1} < g_n$	Releasing	0

independent of the presence of friction. Table 1 enumerates the possible conditions that can arise from algorithmic enforcement of the gap constraints along with the corresponding local contact force values, and a more detailed description can be found in Laursen and Love [11].

Akin to the methods of Jones and Papadopoulos [9], we address Coulomb friction as an analog to algorithmic plasticity, establishing the Coulomb limit as a yield surface. We couch this approach in an Augmented Lagrangian regularization, prescribing a *trial state* $t^{tr}_{T_\alpha}$ as a function of penalty value ϵ_T, the algorithmic gap rate $v^\alpha_{T[n+1/2]}$, and a set of *fixed* multiplier iterates $\lambda^{(k)}_{T_\alpha}$ according to the definition

$$t^{tr}_{T_\alpha} = \lambda^{(k)}_{T_\alpha} + \epsilon_T m_{\alpha\beta[n+1/2]} v^\beta_{T_{[n+1/2]}}. \tag{80}$$

We then determine a trial value for the stick parameter as a function of the trial tangential force magnitudes,

$$\Phi^{tr}_{[n+1/2]} = \left[t^{tr}_{T_\alpha} m^{\alpha\beta}_{[n+1/2]} t^{tr}_{T_\beta} \right]^{1/2} - \mu t_N, \tag{81}$$

and examine the stick–slip criterion through the trial parameter.

IF $\Phi^{tr}_{[n+1/2]} < 0$ THEN (STICK)
we adopt the trial state as the true state, i.e.

$$t_{T_\alpha} = t^{tr}_{T_\alpha}, \tag{82}$$

ELSE (SLIP)
we distribute a Coulomb traction magnitude μt_N according to the relative component sizes of the trial state, i.e.

$$t_{T_\alpha} = \frac{\mu t_N t^{tr}_{T_\alpha}}{\epsilon_T \zeta_{[n+1/2]}}. \tag{83}$$

ENDIF

Substituting the STICK trial case into (77) yields

$$c^l = -\Delta t w^l j^l \left(t_N v_{N_{[n+1/2]}} + \lambda^{(k)}_{T_\alpha} v^\alpha_{T_{[n+1/2]}} + \epsilon_T \zeta^2_{[n+1/2]} \right)^l, \tag{84}$$

similarly for the SLIP trial in (78),

$$c^l = -\Delta t w^l j^l \left(t_N v_{N_{[n+1/2]}} + \frac{\mu t_N \lambda^{(k)}_{T_\alpha} v^\alpha_{T_{[n+1/2]}}}{\epsilon_T \zeta_{[n+1/2]}} \right)^l. \tag{85}$$

It would seem that there is nothing to preclude the possibility of a localized product $\lambda_{\mathrm{T}_\alpha}^{(k)} v_{\mathrm{T}_{[n+1/2]}}^{\alpha}$ from being negative and thus contributing negative dissipation (i.e. generated energy) to a system regularized by Augmented Lagrangians. This condition can only occur, however, in a case where the relative slip velocity $v_{\mathrm{T}_{[n+1/2]}}^{\alpha}$ has reversed direction between iterates of the augmented multiplier, and does not represent a physically viable converged state. It is a trivial algorithmic matter to completely eliminate the possibility of generated energy by setting the multiplier iterate $\lambda_{\mathrm{T}_\alpha}^{(k)}$ to zero whenever it is inappropriately signed relative to the slip velocity, (a situation analogous to zeroing the multipliers on the normal constraints when current values for the contact forces result in separation). With this addendum, the contact formulation will never violate the dissipation criterion (76), and we can be assured that total energy dissipation will be consistent with our discrete a priori estimate upon application of the velocity update.

3.7. Algorithmic summary

The frictional *Velocity Update algorithm* can be summarized as follows.
For each time step $t \in [t_n, t_{n+1}]$:

1. Implicitly solve equilibrium equation (54) for displacements $\boldsymbol{d}_{n+1}$, using an acceptable regularization to enforce the normal and tangential constraints directly, precluding interpenetration in the regularized limit. Identify conditions of STICK or SLIP friction locally according to the regularized description of $\boldsymbol{\Phi}^{\mathrm{tr}}$.
2. Assemble coefficients A^{kl}, b^l, and c^l of the coupled quadratic impulse equation according to the definitions (74), with the allowable contact dissipation determined by (71) in the case of slip friction or set to zero for local stick conditions.
3. Implicitly solve the quadratic impulse Eq. (75) for the contact impulse magnitudes κ^l using an iterative (e.g., Newton–Raphson) solver and following the solution selection criterion outlined in Laursen and Love [11]. Note that consistent-tangent linearizations of (75) are documented in Love [13].
4. Assemble the global contact velocity vector ($\boldsymbol{v}^{\mathrm{c}}$) from the locally defined nodal contributions

$$\boldsymbol{v}_A^{\mathrm{c}} = \sum_{B=1}^{n_{\mathrm{nod}}} M_{AB}^{-1} \sum_{l=1}^{n_{\mathrm{int}}} w^l j^l \kappa^l \left[t_{\mathrm{N}}^l \boldsymbol{N}_{[n+1]_B}^l - t_{\mathrm{T}_\alpha}^l \boldsymbol{D}_{[n+1]_B}^{\alpha l} \right]. \tag{86}$$

   Note that the assembly requires an inversion of the mass matrix.
5. Update the end-state system velocities ($\boldsymbol{v}_{n+1}$) from the displacement and contact velocity values according to the equation

$$\boldsymbol{v}_{n+1_A} := -\boldsymbol{v}_{n_A} + \frac{2}{\Delta t} \Delta \boldsymbol{d}_A + \boldsymbol{v}_A^{\mathrm{c}}. \tag{87}$$

6. Increment $t_n \to t_{n+1}$, Repeat until $t_n = T$.

4. Numerical examples

The following section includes three examples intended to demonstrate the successful extension of the velocity update algorithm to dynamic friction in two and three dimensions, as well as to illuminate the algorithmic distinction between dissipative and conservative behavior given conditions of frictional slip and stick behaviour, respectively. It is to be noted that all examples utilize conservative elastodynamic integration over the interior of each contacting body.

4.1. Dynamic ring impact: Penalty enforced friction

For our first example, we revisit the ring impact problem from Laursen and Love [11], introducing a Coulomb coefficient of friction $\mu = 0.5$ in addition to the material and geometric data listed in Table 2. Two rings are set with initial relative configurations demonstrated by Fig. 1, and the first is given an initial downward velocity in order to initiate an oblique impact in free motion. The contact constraints are enforced by means of a penalty method in both the frictionless and frictional simulation, thus admitting minor penalty-scaled overlaps of the two rings. The limited regularization does not inhibit the energy conservation properties in the fully conservative frictionless case, as noted from the energy graph in Fig. 2(a), and although algorithmic penalty dissipation would be difficult to differentiate from physical dissipation in the frictional case, the partial plot of total energy as calculated without the use of the velocity update routine (included in Fig. 2(b)) indicates that a penalty dissipation is indeed being restored in the updated case, although approximately 5% of the original kinetic energy in the system is being dissipated as

Table 2
Data for ring impact problem

	Ring (1)	Ring (2)	Scaled units
Young's modulus, E	1000	1000	M/[LT^2]
Poisson's ratio, ν	1/6	1/6	–
Density, ρ	0.1	0.1	M/L^3
Material wavespeed, ω	100	100	L/T
Initial velocity, $\boldsymbol{v}_0$	$\{0,-4\}$	$\{0,0\}$	L/T
Center coordinates, $\boldsymbol{x}_0$	$\{0,0\}$	$\{10,-20\}$	L/T
Ring radius, r	10	10	L
Ring thickness, t	0.3	0.3	L
# of circular elements, $n_{\mathrm{el,c}}$	78	78	–
# of radial elements, $n_{\mathrm{el,r}}$	3	3	–
Courant number, Δt_{cr}	$\approx$0.008	$\approx$0.008	T

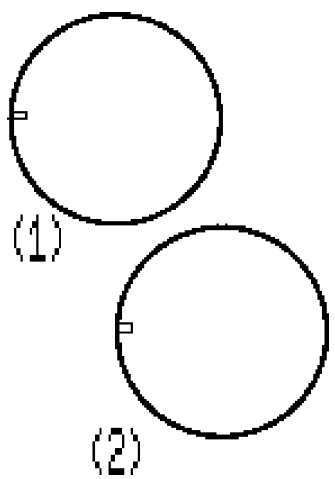

Fig. 1. Ring impact problem, initial configuration.

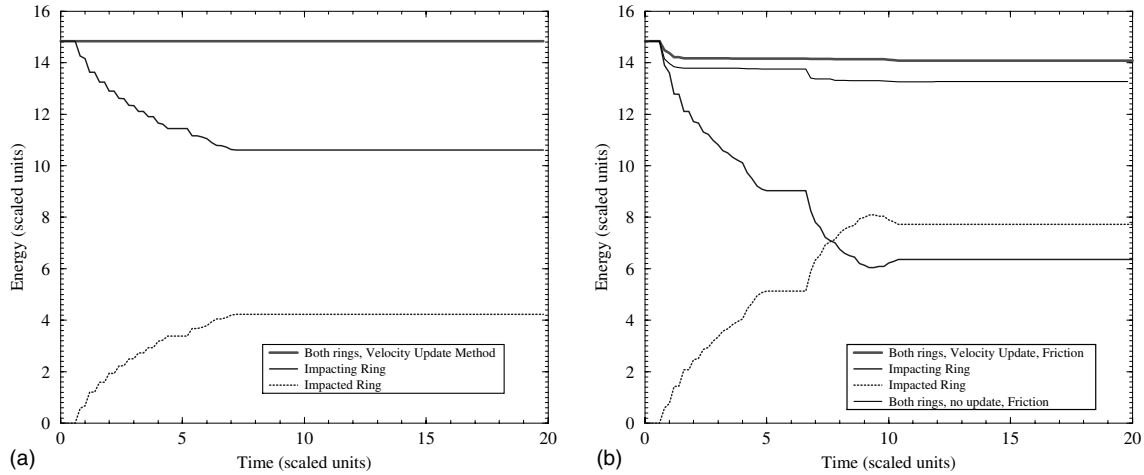

Fig. 2. Ring impact: total energy (a) frictionless and (b) Coulomb friction.

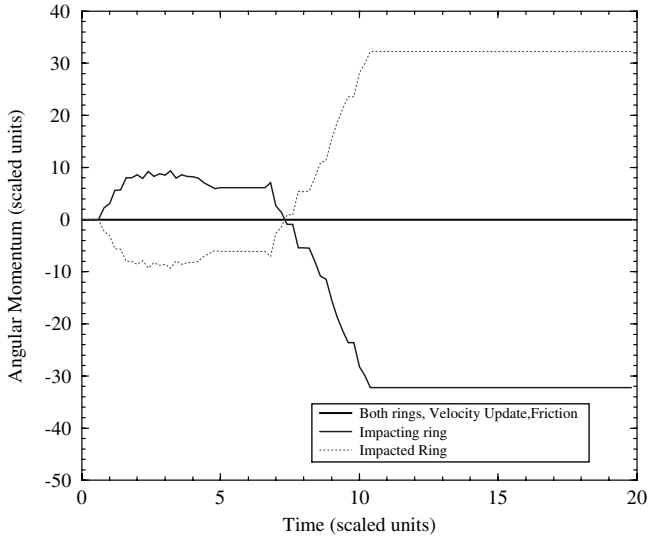

Fig. 3. Ring impact, angular momentum.

a result of slip friction. Note also that Fig. 3 indicates full conservation of angular momentum despite the admitted penalty overlaps.

A sequence of dynamic configurations for the frictional simulation is supplied in Fig. 4, and displays some notable qualitative variations from its frictionless counterpart in Fig. 5. As might be expected, the presence of friction induces a rotational mode in each of the two rings, as evidenced by the relative motion of the tag element. It is also interesting to note that the frictional interface transmits a great deal more of the original kinetic energy from the first ring to the second, as evidenced by the post-contact motions in each simulation and verified by again comparing the energy in each ring in Fig. 2(a) and (b).

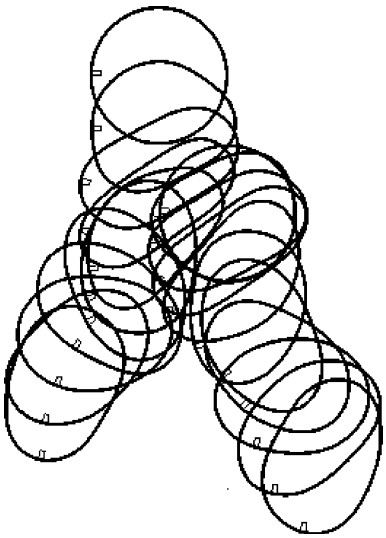

Fig. 4. Friction ring impact, dynamic configurations.

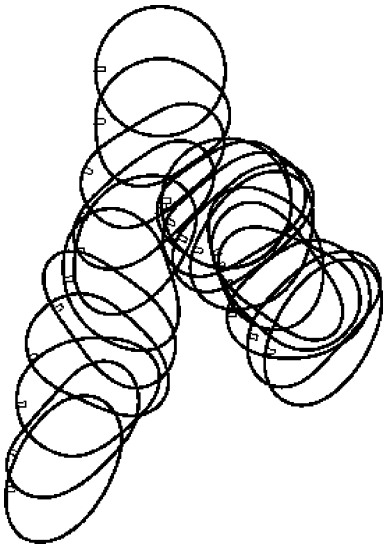

Fig. 5. Frictionless ring impact, dynamic configurations.

4.2. Stick/slip example: Friction blocks

Although relatively contrived, the next example is designed to compare the algorithmic treatment of stick and slip friction. The simulation consists of two three-dimensional elastic blocks (Fig. 6) that impact with relative tangential motion. The base of the larger block is fixed, and the smaller block is given an initial rigid-body velocity that initiates a glancing impact. The larger block initially occupies the cubic space

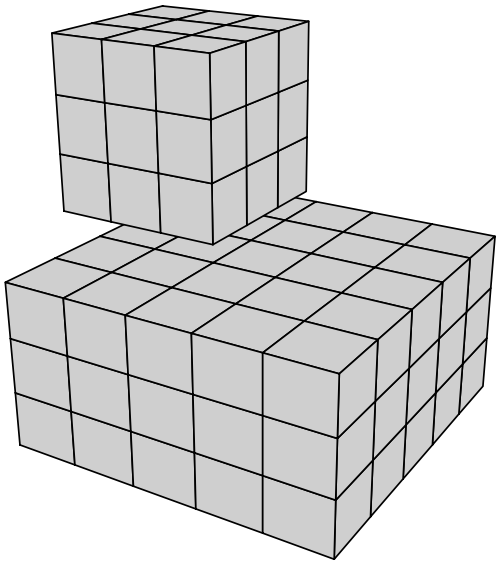

Fig. 6. Friction blocks, initial configuration.

Table 3
Material data for frictional blocks

	Value	Scaled units
Bulk modulus, K	3333	M/[LT^2]
Shear modulus, G	5000	–
Density, ρ	100	M/L^3
Initial velocity, top block, $\boldsymbol{v}_0$	$\{0.0, 1.5, -1.0\}$	L/T

defined by diagonal corner points $\{0, 0, 0\}$ and $\{2.0, 2.0, 1.0\}$ and the smaller block is similarly defined by points $\{0.5, 0.0, 1.25\}$ and $\{1.5, 1.0, 2.25\}$. Table 3 lists the pertinent material data.

Frictional block simulations for both STICK (Coulomb coefficient $\mu = 0.8$) and SLIP (Coulomb coefficient $\mu = 0.2$) are presented in tandem in Fig. 7. In the former case tumbling behavior of the top block is initiated during the first in-contact time step ($t \in [0.2, 0.3]$) due to the stick phenomena, whereas in the latter case, the tumbling behavior is not initiated until a later time step ($t \in [0.6, 0.7]$) when the relative tangential motion has been sufficiently slowed to the stick regime. The energy plots of Figs. 8 and 9 clearly demonstrate the algorithmic conservation of energy for the full stick case and consistent dissipation for slip simulation.

Figs. 8 and 9 also contain, for comparison, simulations run using a Newmark scheme ($\beta = 0.25$, $\gamma = 0.5$) with a similar, albeit non-conserving model for frictional contact. Note that not only is energy dissipated and then numerically created by the Newmark scheme, but the inaccuracies of the scheme also serve to entirely obscure the dissipative effects associated with the change in the frictional coefficient (the changes are minor enough that the graphs appear nearly identical).

4.3. Frictional golf ball simulation

The final example is a more whimsical (although potentially lucrative) one, again taken as an extension of a problem in Laursen and Love [11]. It is well-known among golfers that a well-struck iron shot will

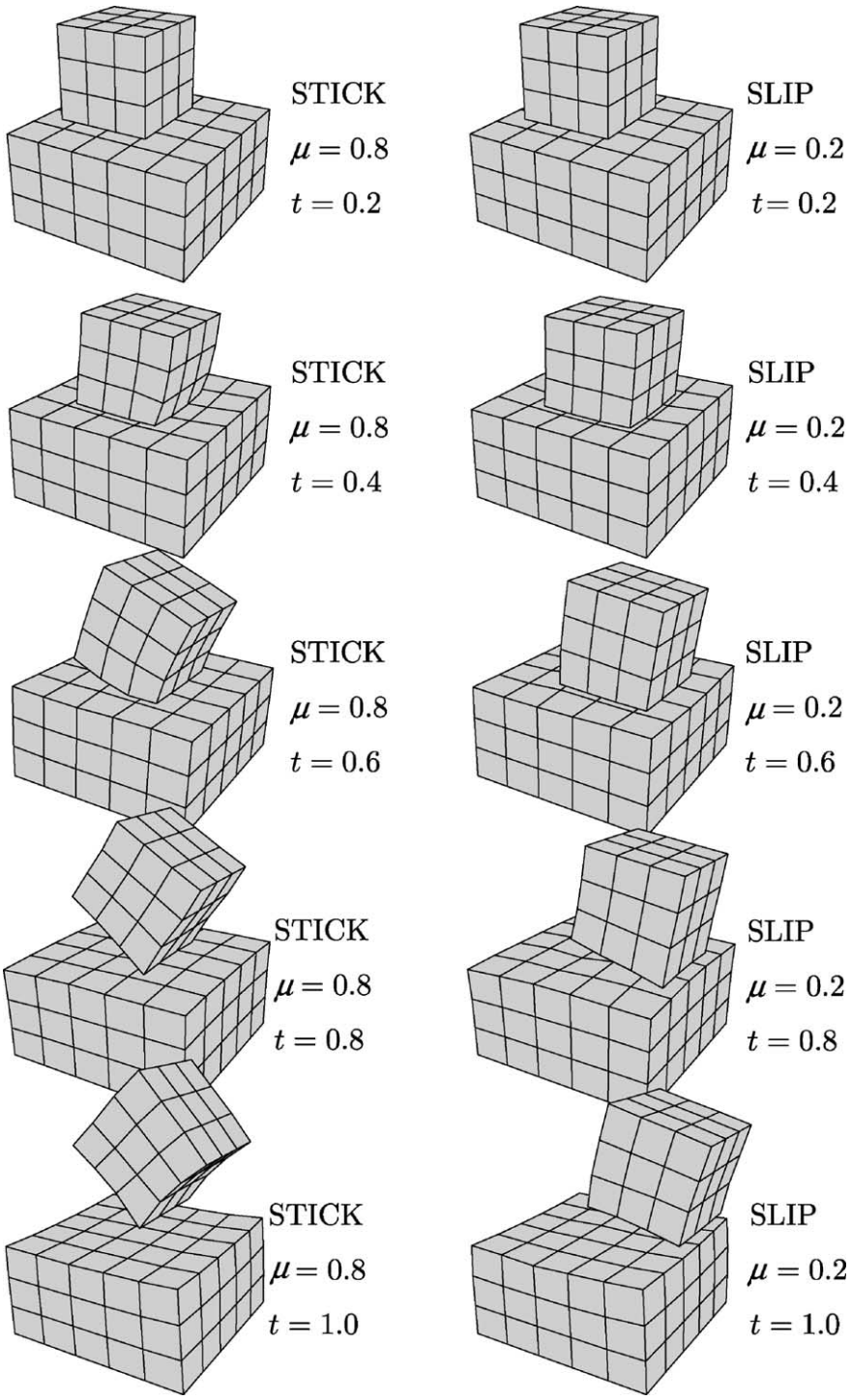

Fig. 7. Frictional block impact, STICK and SLIP simulations.

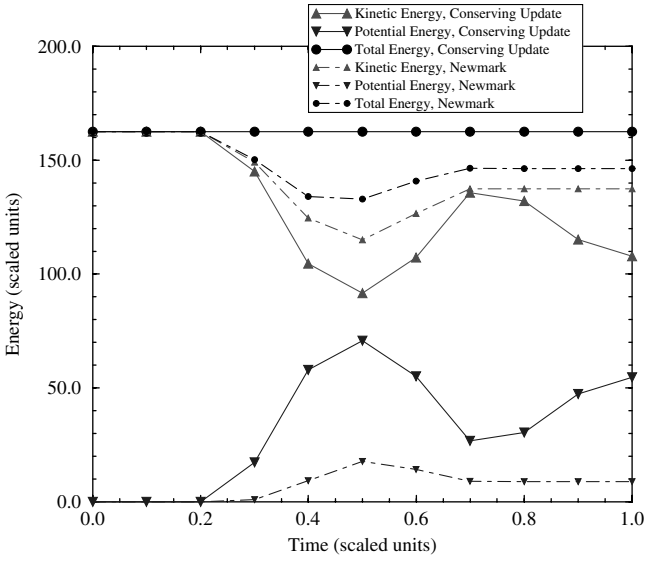

Fig. 8. Frictional block impact: STICK friction energy plot.

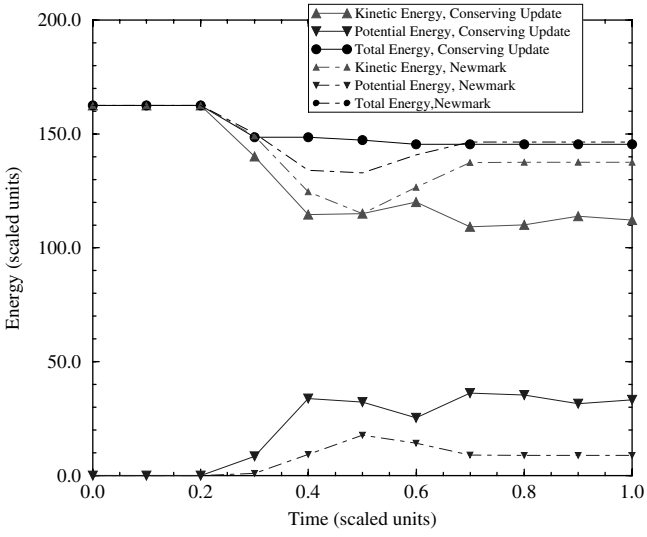

Fig. 9. Frictional block impact: SLIP friction energy plot.

induce backspin on the golf ball, a desirable effect that minimizes rolling of the ball when it lands on the putting green. It is difficult, however, to differentiate between the conditions that promote this spin—on one hand, frictional surface interactions between the dimpled ball and a grooved club face often provide sufficient tangential leverage to induce spin; while in other circumstances, suitably large deformations cause a

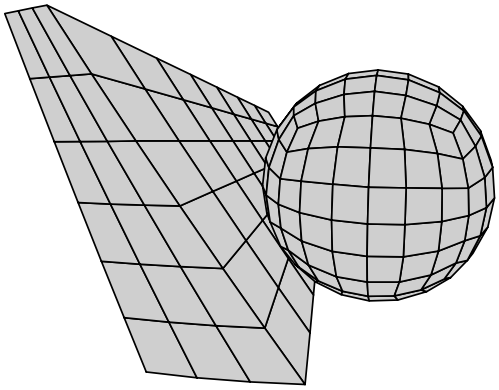

Fig. 10. Golf simulation, initial configuration.

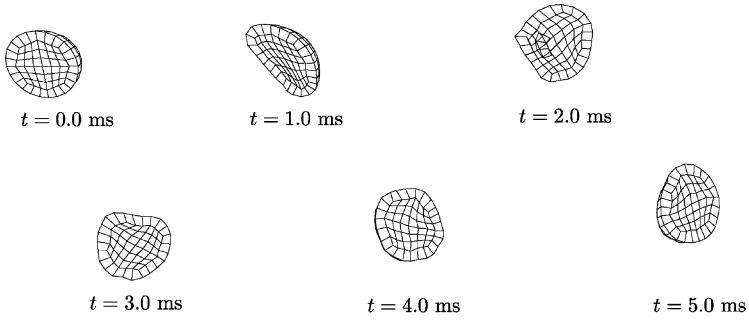

Fig. 11. Frictional golf simulation: cross-sectional ball deformation.

redistribution of golf ball mass such that the spherical symmetry of the ball is broken and normal surface forces can induce spin.

In Laursen and Love [11] we presented frictionless analysis of a ball and club system that failed to produce an appreciable rotation in the simulated golf ball (Fig. 10), belying the second argument somewhat, although the gross simplifications to the material model makes the result far from definitive. (Full material and geometric data for the problem is also included in the original manuscript.) Introduction of an arbitrarily chosen Coulomb coefficient $\mu = 0.5$ does, however, appear to produce the desired effect, as can be observed visually from the series of cross-sectional ball configurations in Fig. 11. Fig. 12 offers more evidence to this effect with a snapshot of the velocity profiles at time $t = 4.0$ ms. The top figure plots the velocity of the ball in the y-plane horizontal to the page, which demonstrates, in conjunction with overall motion to the right (indicated by positive values), also a counterclockwise spin as indicated by the smaller values at the top of the ball and larger values at the bottom. This observation is further confirmed in the bottom figure which similarly plots the velocities, this time in the z-plane vertical with the page, with negative values (down) on the left-hand side and positive values (up) on the right.

The energy plot for the frictional simulation is provided in Fig. 13 and includes the frictionless simulation data for comparison. Approximately 1.2% of the initial system energy is lost due to frictional contact dissipation.

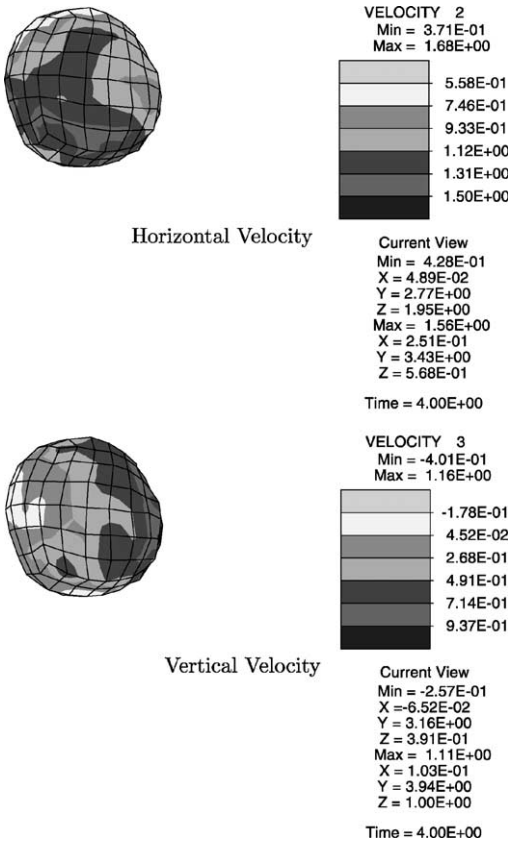

Fig. 12. Frictional golf simulation: velocity spin profiles.

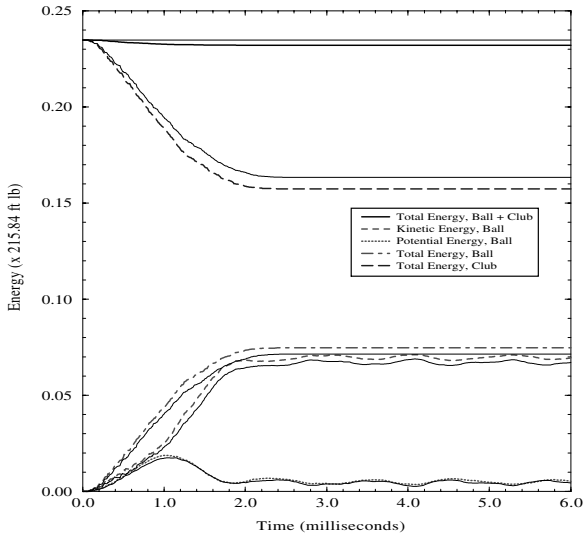

Fig. 13. Golf simulation: frictional and frictionless energy.

5. Concluding remarks

With this manuscript we proffer the *velocity update method* as a complete framework for the treatment of dynamic impact problems. The method makes an accurate accounting of system energy and momenta through the discretization process, thus ensuring proper treatment during numerical simulations and in turn assuring numerical stability. It is designed to accurately reflect the properties of the continuum system, most notably a direct enforcement of the dynamic impact constraints and a localized representation of frictional energy dissipation that discerns conservative stick behaviour from dissipative slip. These properties have been fully implemented for both two and three dimensional systems using both penalty and augmented Lagrangian regularizations. It is our expectation that the velocity update method for the contact interface will be particularly useful in conjunction with energy-consistent methods for dissipative bulk media, where localized energy has a significant effect on deformations.

Acknowledgements

Both authors would like to gratefully acknowledge support given by the Office of Naval Research Young Investigator Program through grant number N00014-97-1-0529; and the National Science Foundation Career Program under grant number CMS-9703356.

References

[1] F. Armero, E. Petocz, A new class of conserving algorithms for dynamic contact problems, Comput. Methods Appl. Mech. Engrg. 158 (1998) 269–300.
[2] F. Armero, E. Petocz, A new dissipative time-stepping algorithm for frictional contact problems: formulation and analysis, Comput. Methods Appl. Mech. Engrg. 179 (1999) 151–178.
[3] F. Armero, I. Romero, On the formulation of high-frequency dissipative time-stepping algorithms for nonlinear dynamics. Part I: low-order methods for two model problems and nonlinear elastodynamics, Comput. Methods Appl. Mech. Engrg. 190 (2001) 2603–2649.
[4] F. Armero, I. Romero, On the formulation to high-frequency dissipative time-stepping algorithms for nonlinear dynamics. Part II: second-order methods, Comput. Methods Appl. Mech. Engrg. 190 (2001) 6783–6824.
[5] V. Chawla, T.A. Laursen, Energy consistent algorithms for frictional contact problems, Int. J. Numer. Methods Engrg. 40 (1998) 863–886.
[6] M.A. Crisfield, J. Shi, A co-rotational element/time-integration strategy for nonlinear dynamics, Int. J. Numer. Methods Engrg. 37 (1994) 1897–1913.
[7] L. Demkowicz, A. Bajer, Conservative discretization of contact/impact problems for nearly rigid bodies, Comput. Methods Appl. Mech. Engrg. 190 (2001) 1903–1924.
[8] O. Gonzalez, Exact energy and momentum conserving algorithms for general models in nonlinear elasticity, Comput. Methods Appl. Mech. Engrg. 190 (2000) 1763–1783.
[9] R.E. Jones, P. Papadopoulos, A yield-limited Lagrange multiplier formulation for frictional contact, Int. J. Numer. Methods Engrg. 48 (2000) 1127–1149.
[10] T.A. Laursen, V. Chawla, Design of energy conserving algorithms for frictionless dynamic contact problems, Int. J. Numer. Methods Engrg. 40 (1997) 863–886.
[11] T.A. Laursen, G.R. Love, Improved implicit integrators for transient impact problems—geometric admissibility within the conserving framework, Int. J. Numer. Methods Engrg. 53 (2002) 245–274.
[12] T.A. Laursen, J.C. Simo, A continuum-based finite element formulation for the implicit solution of multibody, large deformation frictional contact problems, Int. J. Numer. Methods Engrg. 36 (1993) 3451–3485.
[13] G.R. Love, Velocity update algorithms for transient impact problems: consideration of kinematic discontinuities within a conserving framework, Ph.D. dissertation, Duke University, 2000.
[14] X.N. Meng, T.A. Laursen, Energy consistent algorithms for dynamic finite deformation plasticity, Comput. Methods Appl. Mech. Engrg. 191 (2002) 1639–1675.

[15] J.C. Simo, T.A. Laursen, An augmented lagrangian treatment of contact problems involving friction, Comput. Struct. 42 (1992) 97–116.
[16] J.C. Simo, N. Tarnow, The discrete energy–momentum method. Part I. conserving algorithms for nonlinear elastodynamics, Z. Angew. Math. Phys. 43 (1992) 757–793.